



Steering single-site metallaphotocatalytic pathway by accumulated electron on carbon nitride support

Bangrong Ming ^{a,b}, Tongtong Jia ^{a,b}, Yufan Zhang ^{a,b}, Jikun Li ^{a,b}, Chuncheng Chen ^{a,b}, Wenjing Song ^{a,b,*}, Jincai Zhao ^{a,b}

^a Key Laboratory of Photochemistry, CAS Research/Education Center for Excellence in Molecular Sciences, Institute of Chemistry, Chinese Academy of Sciences, Beijing 100190, PR China

^b University of Chinese Academy of Sciences, Beijing 100049, PR China



ARTICLE INFO

Keywords:

Heterogeneous photocatalysis
Single-site nickel
Organic halide
Carbon nitride
Electron accumulation

ABSTRACT

Organic halide transformation is of high importance for fine chemical synthesis and environmental remediation. Integrated photocatalytic platforms open up distinctive reaction pathway for carbon-halogen bond activation/reconstruction. Herein we reveal carbon nitride (CN)-ligated single atom nickel (Ni_1/CN), with accumulated electron on the CN, paves Ni-mediated electron-proton transfer, enabling hydrodehalogenation, along with the catalytic carbon–oxygen (C–O) coupling. The preference for hydrodehalogenation positively correlates with density of electron on CN. EPR measurements suggest photo-generated Ni^{i} interacts with aryl halides, followed by electron transfer or reductive elimination to give different products. Further kinetic studies on hydrodehalogenation/C–O coupling show the reaction orders of 0.1/0.5 in aryl halide and 1.5/0.03 in (CN) electron, unveiling rate-determining step as oxidative addition to Ni^{i} and (CN) electron transfer for the two conversions. Our work advances in modulating aryl halide conversion by carrier accumulation on the photoactive support and guides metallaphotocatalytic platform design/operation toward target transformations.

1. Introduction

The cooperation of transition metal catalysts with light-harvesting photosensitizers opens up unique reaction paradigms to achieve challenging transformation powered by light [1–4]. An important implementation of this approach is turning on transition metal (e.g., Ni polypyridyl complexes or Cobalamin) catalytic cycles for the target transformations of organic halides, including cross-coupling or hydrodehalogenation for elimination of halogenated contaminants and synthesis of value-added building blocks [5–9]. Typically, the excitation of a photosensitizer (noble metal complexes, organic dyes or semiconductors) induces electron/energy transfer to give low-valence species ($\text{Ni}^{1/0}$, Co^{i}) or excited states of the metal catalysts, which dissociate carbon-halogen bonds; the follow-up steps, such as halide-nucleophile exchange-reductive elimination or photolysis of metal intermediate, furnish different products [10–14]. The selection of photosensitizers, as well as the sensitizer/catalyst organization, are fundamental to orchestrate electron/energy transfer, defining reaction patterns and catalytic

performance [15–19]. In this regard, incorporation of isolated metal site in the matrix of photoactive materials, offers new opportunity to regulate charge/energy transfer, bond activation/reconstruction pathways and thereby catalytic activities [20–22].

Recently, our group and several others [23–26] have developed single-site Ni catalyst, with Ni^{2+} coordinated to nitrogen sites of the light-harvesting carbon nitride (Ni_1/CN), as novel metallaphotocatalytic platform. In this architecture, the Ni-N moiety functions as the classic polypyridyl Ni complexes, catalyzing light-driven reaction of organic halides with various nucleophiles (alcohol, carboxylic acid, or amines) [6,23–26]. The intra-framework electron transfer and the isolated Ni sites bring outstanding atomic efficiency and structural integrity suitable for sustainable operation (no aggregation/deactivation) [11,25, 27]. Despite of these successes, less is known about the catalytic activate species, or the key elemental steps in these single-site photocatalysts. Also it is worth to note that the photoactive CN support is an unique electron (proton) reservoir: under irradiation in the presence of hole scavengers (conditions relevant for organic halide's transformation), the

* Corresponding author at: Key Laboratory of Photochemistry, CAS Research/Education Center for Excellence in Molecular Sciences, Institute of Chemistry, Chinese Academy of Sciences, Beijing 100190, PR China.

E-mail address: wsongunc@iccas.ac.cn (W. Song).

semiconducting CN support, which features an exponential energetic distribution of trap states below conduction band [28–30], is capable of storing electrons in these trap state (accompanied by the adsorption of the charge-compensating protons) [28,31]. We envision that the electron accumulation on CN (determined by irradiation conditions) would impact electron transfer process and the transformation of organic halide.

Herein, by mapping performance of Ni_1/CN under designed conditions, we uncovered the catalytic hydrodehalogenation in addition to the previously established C–O coupling in aryl halide-alcohol reaction ($\text{ArBr} + \text{CH}_3\text{OH} \rightarrow \text{ArH} + \text{ArOCH}_3$). Preference toward C–O coupling or hydrodehalogenation depends on concentration of halogenated substrate, and/or density of available electron on CN regulated by photon flux/energy. EPR measurements and control experiments with pre-irradiated catalyst suggested the involvement of photogenerated Ni^{I} and (CN) electron in Ni_1/CN catalysis. In combination with distinct rate law of the two conversions, a mechanism is proposed, including the rate-limiting oxidative addition (followed by reductive elimination, OA/RE) toward coupling, and photo-promoted Ni mediated (proton coupled) electron transfer enabled hydrodehalogenation.

2. Experimental section

2.1. Chemicals

Triethylamine (TEA) (99.5 %), sodium hydroxide (NaOH) (99 %), urea (99 %), acetophenone (99 %), 4-methoxyacetophenone (98 %), 4-bromoacetophenone (98 %), 4-bromobenzonitrile (98 %), benzonitrile (99 %), bromobenzene (99.5 %), 1,4-dibromobenzene (98 %), 4-bromoanisole (98 %), 1-bromo-4-(trifluoromethyl)benzene (99 %), anisole (99 %), 1,4-dimethoxybenzene (99 %) were purchased from Innochem Co., Ltd. (Beijing, China). All chemicals were used without further purification. $\text{NiCl}_2 \cdot 6 \text{ H}_2\text{O}$ (99.95 %, Alfa Aesar), CH_3OH (chromatographic grade, CONCORD), CH_3OD (99.5 %, J&K), CD_3OH (99.5 %, J&K), 4-bromoacetophenone (98 %, Alfa Aesar), 4-methoxybenzonitrile (98 %, Energy Chemical), 4-(trifluoromethyl)anisole (98 %, Alfa Aesar) and (trifluoromethyl)benzene (99 %, J&K) were used as received.

2.2. Preparation of Ni_1/CN

Graphitic carbon nitride ($\text{g-C}_3\text{N}_4$ or CN) was prepared by pyrolysis of urea. In a typical synthesis, 20 g urea was put into a covered crucible and calcined in a muffle furnace at 600 °C for 4 h (ramp rate 5 °C/min). CN ligated atomically dispersed nickel (Ni_1/CN) was synthesized by a microwave-irradiation-assisted deposition method. Typically, 100 mg CN was mixed with 5 mg of $\text{NiCl}_2 \cdot 6 \text{ H}_2\text{O}$ in 7.5 mL of acetonitrile. Then 65 μL of TEA was added, and the mixture was stirred for 1 h. The capped vessel was placed in MCR-3 microwave reactor and was subjected to 80 °C treatment for 2 h. After the microwave treatment, the resulting precipitate was recovered by filtration, and was washed twice with chloroform, methanol and acetonitrile. The collected Ni_1/CN solid was vacuum-dried overnight at 80 °C.

2.3. Characterization

The Fourier transform infrared (FTIR) spectra were recorded on a BRUKER spectrometer (VERTEX 70 v). X-ray diffraction (XRD) was conducted on an X-ray diffractometer (Empyrean) with Cu-K α radiation at ambient temperature and pressure. The steady-state photoluminescence was measured on a fluorescence spectrometer (F-7000) under 365 nm excitation. Time resolved photoluminescence decay spectra were measured on Hamamatsu C11367 Quantaurus-Tau to obtain fluorescence lifetime. The UV-Vis diffuse-reflection spectra (DRS) were recorded on a Shimadzu UV-vis spectrophotometer (UV-3900). The Ni content was quantified by an inductively coupled plasma mass spectrometry (ICP-MS) (Thermo iCAP RQ). X-ray photoelectron

spectroscopy (XPS) was conducted on an electron spectrometer (Thermo ESCALAB250XI) with a Mg K α (1253.6 eV) source. All binding energies were calibrated against the C 1s peak at 284.8 eV. High-resolution transmission electron microscopic (HR-TEM) images and energy-disperse X-ray (EDX) elemental mapping images were obtained on a JEM-F200 transmission electron microscope (JEOL, Japan). Aberration-corrected high-angle annular dark field scanning transmission electron microscopy (AC-HAADF-STEM) images were obtained on a JEM ARM200F. X-ray absorption spectra were collected at the 1W1B beamline at Beijing Synchrotron Radiation Facility (BSRF). The radiation was monochromatized by a Si (111) double-crystal monochromator. X-ray absorption near edge structure (XANES) was collected in the fluorescence mode. The Ni foil extended X-ray absorption fine structure (EXAFS) was measured with a reference ion chamber for energy calibration for each sample. XANES and EXAFS data analysis were processed by Athena software. X-band electron paramagnetic resonance (EPR) spectra were collected on an E500 spectrometer at 90 K (Bruker, Switzerland). Gas chromatography-mass spectrometry (GC-MS) analysis was obtained on an Agilent 7890 gas chromatograph system with an electron ionization (EI) mass spectrometer (HP-5 column, 30 m \times 320 μm \times 0.25 μm). The molecular structure was directly acquired from the equipped analytical software.

2.4. Photochemical measurements

Generally, 10 mg of Ni_1/CN , 0.005 - 0.5 mmol of aryl bromide substrate and NaOH (2 equiv of aryl bromide or 0.2 M) were added to 5 mL of CH_3OH . The suspension was purged with argon to remove oxygen under magnetic stirring in the dark for at least 15 min. Photoreaction was carried out by a 420 nm LED irradiation (100 mW cm^{-2}). The temperature was kept at 40 °C by a thermostat. The irradiation time was 6 h unless otherwise noted. The products were monitored by GC or HPLC.

3. Results and discussion

3.1. Ni_1/CN catalyst

Ni_1/CN was prepared by a previously reported method with slight modifications [32]. The XRD and FT-IR results (Figs. S1a-b) display the characteristic diffraction peaks of (100) interplanar packing of heptazine units and the (002) π – π interlayer stacking at 13.0 and 27.3 °, and typical vibration band of CN in 810, 1200 to 1600, and 3000 cm^{-1} region [29], confirming the maintenance of structural features of carbon nitride in Ni_1/CN . The selected catalyst contained 0.7 wt% of Ni as determined by ICP-MS. The transmission electron microscopy and the energy dispersive X-ray spectroscopy (EDX) revealed homogeneously distributed Ni in the matrix of carbon and nitride (Fig. S2a). The isolated Ni sites in the fresh and recycled Ni_1/CN were further identified by aberration-corrected high-angle annular dark-field scanning transmission electron microscopy (AC-HAADF-STEM) (Fig. 1a and Fig. S2b), confirming Ni maintained the isolated form after catalysis. The X-ray photoelectron spectrum of Ni_1/CN , featuring $\text{Ni} 2\text{p}_{3/2}$ (856 eV and the satellite peak at 862 eV) and $\text{Ni} 2\text{p}_{1/2}$ (873 eV and the satellite peak at 880 eV) peaks, suggests an oxidation state of + 2 for Ni (Figs. S1c-d) [23]. This is also consistent with result of the X-ray absorption near edge structure (XANES) of Ni_1/CN showing an edge energy close to that of NiO (Fig. 1b) [23]. The extended X-ray absorption fine structure (EXAFS) (Fig. 1c and Fig. S4) resolved a dominant peak centered at 1.56 Å, which can be assigned to Ni–N/C scattering in the first coordination sphere [20,33,34]; the typical Ni–Ni contribution at 2.13 Å is absent and these structure features maintains in the EXAFS of the recycled catalyst (Fig. S3). The wavelet transformed (WT) EXAFS spectra of Ni_1/CN , together with reference Ni samples (Fig. 1e) showed the position of the main maximum of Ni_1/CN dominated at k-value of c.a. 4.3 Å $^{-1}$ and R-value of c.a. 1.5 Å, which is similar to that of Ni–N contribution in

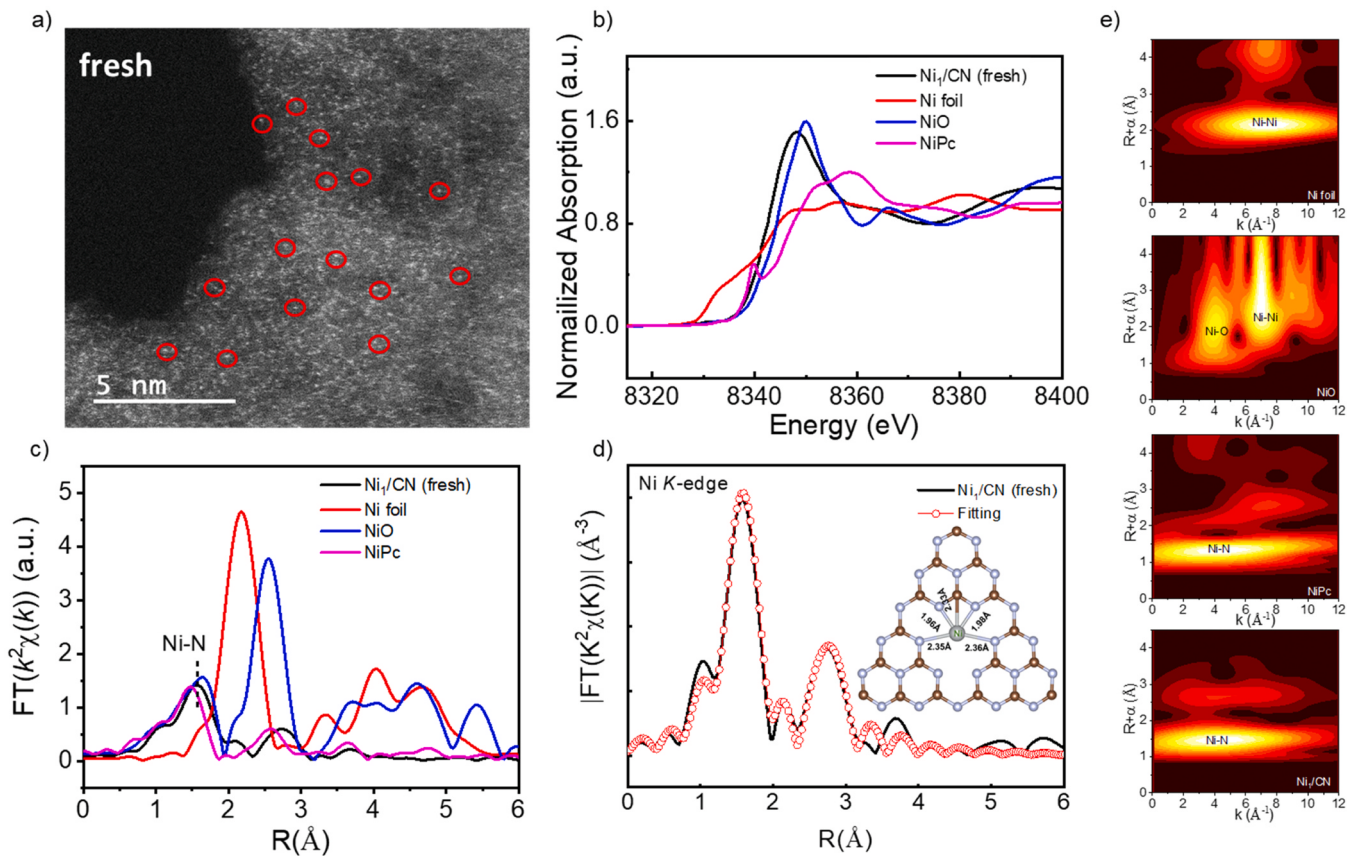


Fig. 1. (a) HAADF-STEM image of Ni₁/CN (the selected isolated Ni sites are visually guided by red circles). (b) Normalized XANES spectra, and (c) k^2 -weighted Fourier transform of the EXAFS spectra at the Ni K-edge with reference to Ni foil, NiO, and NiPc. (d) EXAFS fitting of Ni₁/CN at the R space (inset shows the structure of the nickel site in Ni₁/CN; the balls in brown, baby blue, and grey represent C, N and Ni atoms, respectively). (e) Wavelet transformed EXAFS spectra of Ni foil, NiO, NiPc and Ni₁/CN.

NiPc; the second WT-EXAFS peak at a similar k-value (4.2 Å⁻¹) has a maximum R-value of ca. 2.7 Å, associated with photoelectron interactions with low Z elements (N, C, or O) or a result of multiple scattering events within the first coordination shell. Based on a fitted coordination number of 4.9 (Table S1), a configuration of Ni coordinated to four (CN) pyridinic nitrogen, and one (CN) heptazine carbon is proposed (Fig. 1d inset) [35]. Anchoring of Ni²⁺ quench the steady state photoluminescence (PL) of CN and reduce the PL lifetime (Fig. S4), indicative of photoinduced electron transfer from CN to single-site Ni²⁺.

3.2. Ni₁/CN catalyzed aryl halide-alcohol reaction

Using the reaction of 4-bromobenzonitrile (**1**) with methanol as a model, the performance of Ni₁/CN was tested under different conditions. Methanol was used as solvent for simplification. Photocatalytic reactions with 2 g L⁻¹ of Ni₁/CN under 6 h 420 nm irradiation led to production of both C–O coupling product 4-methoxybenzonitrile (**2**) and dehalogenated product benzonitrile (**3**). The temporal profiles manifested the concurrent formation of **2** and **3** without crossover or sequential conversion (Fig. S5a). The indispensability of single-site Ni–N on CN is confirmed by the control experiments (Table S2): the transformation of **1** gave similar result in another single site Ni_{SAC}/CN catalyst with lower Ni; the reaction does not proceed in pristine CN. In addition, the hydrogen incorporated in **3** was evidenced to originate from the hydroxyl group rather than the methyl of methanol by isotope labelling (i.e., reaction in CD₃OH or CH₃OD, Fig. S6), which argues against hydrodehalogenation pathway via hydrogen abstraction of aryl radical, the typical mechanism in photocatalysis or dual Ni/photoredox catalysis [18,36]. The yields and product distribution (assessed by yield

ratio [3]/[2] after 6 h reaction) changed with concentration of **1** (with either constant 0.1 M NaOH, or 2 equiv of **1**, Fig. 2a-b and S5b). Specifically, preference toward C–O coupling/hydrodehalogenation was found in high/low concentration regimes of **1**. As shown in Fig. 2a (detailed in Table S3), at 0.1 M of **1**, the yields of **2** and **3** were 54 % and 20 %, respectively; at a decreased concentration of **1** (0.02 M), a preference for hydrodehalogenation was observed, producing 37 % of **2** and 41 % of **3**; while 10 % of **2** and 68 % of **3** were formed at 1 mM of **1**, corresponding to change in [3]/[2] from 0.36 to 3.8. We assessed the catalyst's activity in three catalytic runs, the catalyst remained active for both conversions after 6 h photoreaction (Fig. S7). In addition, similar dependencies of the two products' yields ratio on substrate concentration were observed for other selected aryl halides (4-bromoacetophenone, 1-bromo-4-(trifluoromethyl) benzene and 1, 4-dibromobenzene, Fig. 2c). Such phenomenon indicates different reaction order in aryl halide for coupling and dehalogenation, which will be discussed in detail in the following section.

As discussed in the Introduction, irradiation condition may affect halogenated substrate transformations by electron accumulation/transfer on CN. Indeed, the reaction profile demonstrates a strong dependency on irradiation conditions. As shown in Fig. 2d, yield of **3** enhanced from 25 % to 45 % with light intensity (25 to 100 mW cm⁻², 420 nm), while C–O coupling was less affected (38–42 %), corresponding to products' yield ratio ([3]/[2]) increased from 0.7 to 1.2 with light intensity. The reaction under different wavelengths was further examined, and the normalized yield of **2** or **3** (the yield after 1 h reaction was divided by responding photon flux) was obtained (Fig. 2e). The hydrogenation yield matched well with the absorption feature of Ni₁/CN, while that of **2** maintained at a similar level from 395 to 470 nm,

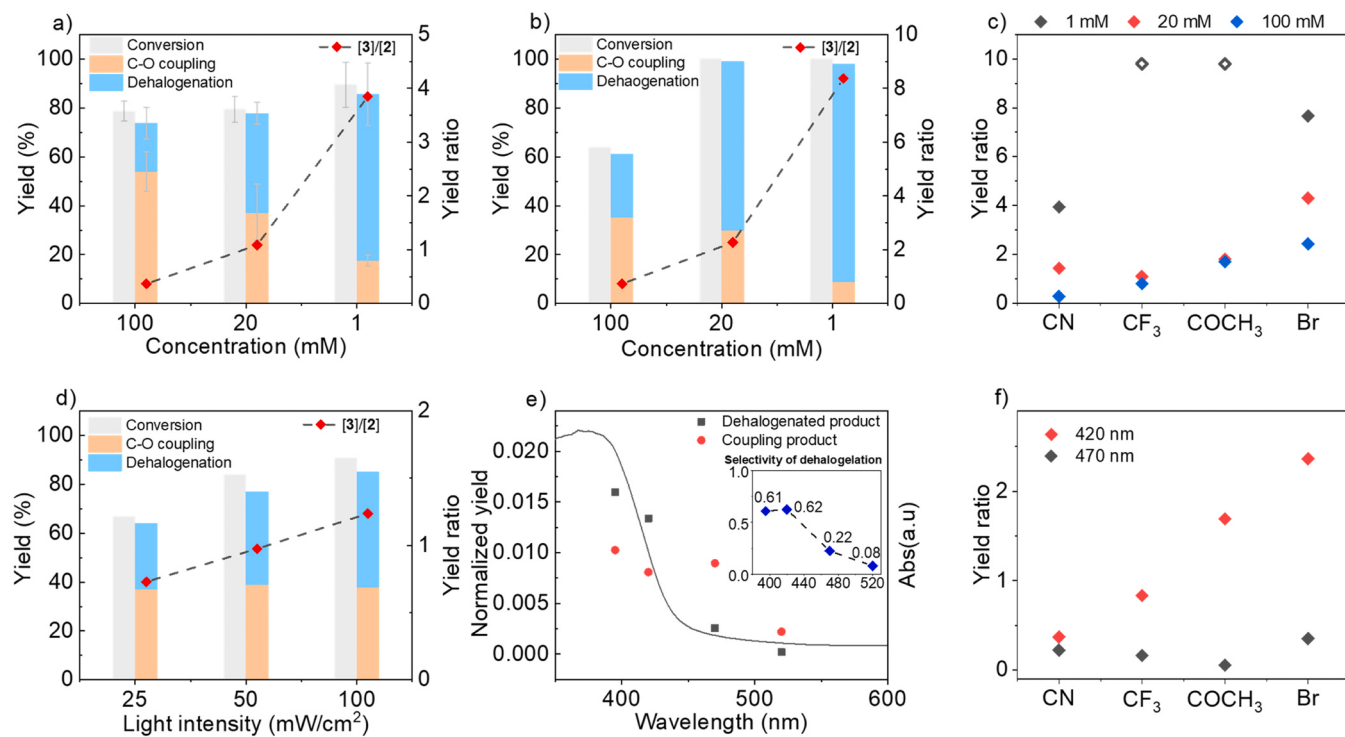


Fig. 2. Aryl halide-methanol reaction catalyzed by Ni_1/CN . Conversion of **1** (gray) and yield of the **2** (orange) **3** (blue) under various 4-bromobenzonitrile concentration with (a) 2 equivalent NaOH (Error bar from three tests was given) and (b) 0.2 M of NaOH; (c) Hydrogenation/coupling products' ratios ($[3]/[2]$) found for other substrates with varied concentration (The hollow symbol represents only hydrodehalogenation product was detected). (d) Conversion of 20 mM **1** (gray) and yield of the **2** (orange) and **3** (blue) under 420 nm irradiation at various intensities. (e) The 1 h yields of **2** (black squares) and **3** (red circles) in 20 mM **1** normalized by photo flux under different wavelengths (left, normalized yield = $N_x/(P * t * \lambda / N_A h c)$, N_x -mole number of product/mol, P -light intensity/W cm^{-2} , λ -wavelength/m, t -time/s, N_A -Avogadro constant/mol $^{-1}$, h -Planck constant/J·s, c -speed of light/m s^{-1}), overlaid with the diffusion-reflection absorption spectrum of Ni_1/CN (right); inset, the dehalogenation selectivity under different wavelengths. (f) Yield ratio of hydrogenation/coupling found for other substrates (0.1 M) with 420 nm or 470 nm irradiation for 6 h. Conditions: Ni_1/CN (10 mg), NaOH (0.2 M) in 5 mL of CH_3OH at 40 °C under Ar.

displaying an inverse in conversion/selectivity between 450 and 470 nm (Fig. 2e inset). The more pronounced change in hydrodehalogenation than that of C-O coupling with irradiation conditions is also observed in reaction of other aryl bromides with methanol, particularly for aryl bromides with weaker electron-withdrawing group at the para position (Fig. 2f). In addition, when water was used as the coupling partner, similar changes in hydroxylation/hydrodehalogenation with irradiation condition was observed (Fig. S8).

3.3. The involvement of photogenerated Ni^{I} and electron in Ni_1/CN catalyzed coupling and dehalogenation

Interestingly, reaction of 20 mM **1** with pre-irradiated Ni_1/CN suspension produced both **2** and **3** in the dark, albeit at very low amounts (0.43 μmol of **2** and 0.45 μmol of **3**); the yield of **2** increased with concentration of **1** but the yield of **3** almost unchanged (Fig. S9). Such results imply the accumulation of photo-generated active species that are capable of converting substrate to both products. To track the

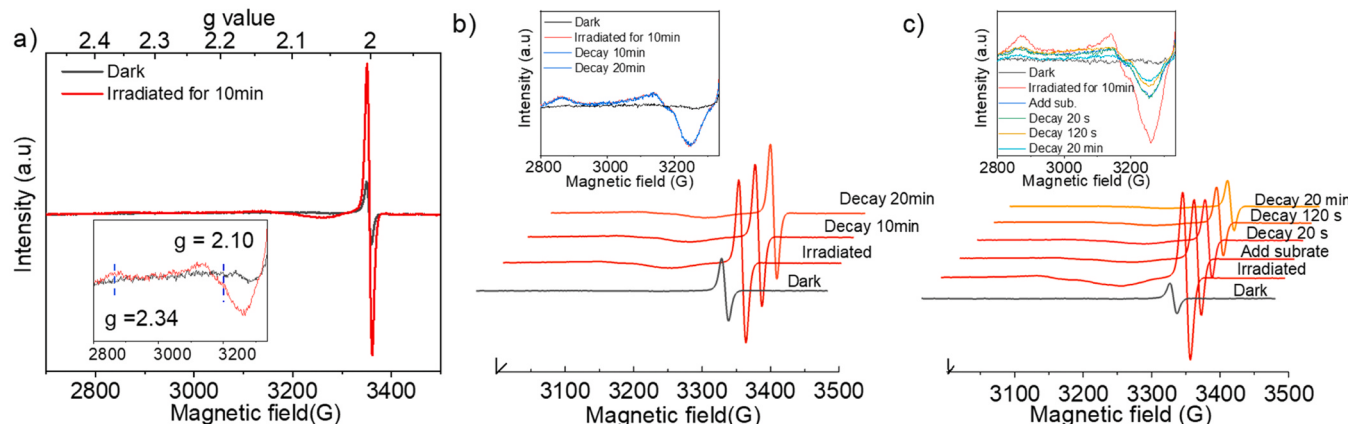
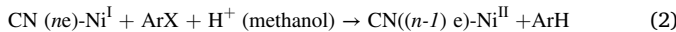


Fig. 3. EPR spectra of Ni_1/CN suspension in methanol after indicated treatment. (a) The Ni_1/CN suspension before (gray) and after 10 min of 420 nm irradiation under Ar (red). Time-resolved EPR spectra of Ni_1/CN collected under Ar (b) after irradiation for 10 min or (c) after addition of **1** (0.1 M) into the irradiated Ni_1/CN . Inset, enlarged area showing the corresponding signal of monomeric Ni^{I} . (The addition was proceeded in a glove box at R.T., then the sample was immediately cooled in a liquid N_2 Dewar for EPR measurement.) X-band ($\nu = 9.4$ GHz), microwave power: 2.0 mW, modulation amplitude: 10 G, detection temperature: 90 K.

evolved species in Ni_1/CN upon irradiation, EPR spectra of catalyst dispersion in methanol were collected at 90 K (Please find the experimental details in the [Supplementary Material](#)). As shown in [Fig. 3a](#), Ni_1/CN displays a signal at $g = 2.004$ assigned to (CN) electrons localized at C 2p orbital of CN [37], and it enhances pronouncedly after 10 min of illumination, arising from the accumulation of photo-generated electrons on CN (hole was consumed by methanol) [38]. In the meantime, another anisotropic signal with $[g_{xx}, g_{yy}] = [2.34, 2.10]$ appears ([Fig. 3a](#), the g_{zz} value cannot be satisfactorily obtained due to the interference from electron signal), which is typical for a monovalent Ni^{I} species with an unpaired d_{xy}^2 electron [39–41]. Both signals were stable for at least 20 min under Ar atmosphere ([Fig. 3b](#)).

Upon airproof addition of 0.1 M **1** to the irradiated Ni_1/CN , intensity of (CN) electron ($g = 2.004$) reduced by 30 %, and the anisotropic signal assigned to Ni^{I} species also dropped by 50 % ($g = 2.34$) ([Fig. 3c](#) and inset) immediately; and both signals gradually decayed to below 20 % of the initial intensity within 20 min (the residue signal is tentatively assigned to less-reactive Ni^{I} [11]). The hydrodehalogenation and coupling products were also found in the tested thawed EPR suspension ([Fig. S9a](#)). These results suggest the reaction of aryl halide with the accumulated photo-induced electrons and $\text{Ni}^{\text{I}}(\text{N})$. To follow the photo-generated electron participated process, in-situ EPR experiment was performed at R.T.: the electron signal in presence of **1** barely increase compared to the suspension without **1** ([Fig. S10](#)). It is proposed earlier that Ni^{I} can activate carbon-halogen bond to initiate redox neutral OA/RE cycle (with no external reducing equivalent) to afford C–O coupling product [11,42–45]. Here, the electron consumption with pre- or post-addition of **1** ([Fig. 3c](#) and S10), and formation of **3**, imply an electron transfer enabled hydrodehalogenation. Furthermore, the hydrodehalogenation does not occur via single electron transfer-hydrogen atom abstraction (ruled out by hydrogen source in [Section 3.1](#) and the absence of radical in the trapping experiments, Figs. S11 and S12) [46,47]. Taking the necessity of Ni into account, the light-driven hydrodehalogenation is most consistent with a Ni mediated electron–proton transfer ([Eq. 1–2](#)).



3.4. Correlation between preferences for hydrodehalogenation with photo-modulated available/transferrable electron on CN

Recognizing the relevance of Ni_1/CN catalyzed hydrodehalogenation to the photo-accumulated electrons on CN, we turn to quantify the relationship between available electrons on CN and reaction products in Ni_1/CN catalysis. The density of photogenerated electron available for reductive reaction under various conditions were assessed independently by using Fe^{3+} as the electron acceptor ([Fig. S13](#)) [48]. In the first 20 min of irradiation, reduction of Fe^{3+} displayed a zero-order kinetics ([Fig. S13a](#)), which allowed us to extract the density of transferable electron (N_e) on Ni_1/CN , ranging from 0.055 to 0.32 $\mu\text{mol mg}^{-1}$ under different light intensities (25 to 100 mW cm^{-2} , 420 nm) or wavelengths (470 and 520 nm at 100 mW cm^{-2}) ([Fig. S13b](#)). The yield of **3** (6 h) is positively correlated to available/transferrable electron on Ni_1/CN ([Fig. 4](#)), reinforcing the role of CN support, by accumulating/transferring electrons, in directing the Ni_1/CN catalyzed organic halide conversion.

3.5. Rate law analysis and key steps in Ni_1/CN photocatalysis

To gain further insight into the two conversions, we investigated the reaction kinetic features. Under different initial concentration of **1**, the initial rates (r) of C–O coupling and hydrodehalogenation ([Fig. S14](#))

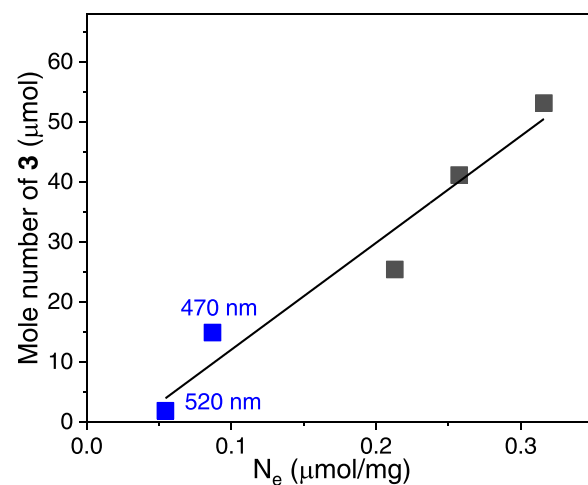


Fig. 4. The production of **3** after 6 h reaction in 20 mM **1** was plotted against available electron density (N_e , 10 min) estimated from photogenerated Fe^{2+} under indicated irradiation conditions (420 nm at 25, 50 and 100 mW cm^{-2} 470 nm and 520 nm at 100 mW cm^{-2}).

were used to extract the reaction order (α) in halogenated substrate and the rate constants by [Eq. 3a–b](#) (k_{H}' or $k_{\text{C–O}}'$, which include the contribution from the electron term in [Eq. \(3\)](#)). As shown in [Fig. 5a](#), the coupling process displays a fractionally positive order of c.a. 0.5 in **1**, similar to those reported dual Ni/carbon nitride catalyzed coupling reaction [25,49]. Hydrodehalogenation is, however, not sensitive to **1**, displaying a reaction order below 0.1. The rate constants, k_{H}' and $k_{\text{C–O}}'$, are 0.0069 $\text{mM}^{0.5} \text{ min}^{-1}$ and 0.043 $\text{mM}^{0.9} \text{ min}^{-1}$ under 100 mW cm^{-2} 420 nm illumination (the fraction unit of rate constant in concentration was calculated from reaction order as $1-\alpha$). Under 100 mW cm^{-2} 470 nm illumination ([Fig. S15](#)), k_{H}' is one magnitude lower than that at 420 nm, while the $k_{\text{C–O}}'$ decreases by 48 %; but the change of order (α) in **1** is non-significant ([Fig. 5b](#) and [Fig. S15](#)). Such changes in rate constant manifests the different contributions of electron term (described by β , [Eq. \(3\)](#)) to the production of two products. Since electron is not a standard reagent like **1**, β was alternatively derived by reaction progress kinetic analysis (RPKA) using the two datasets of rate collected at 420 nm and 470 nm ([Eq. 3c](#). Please see the [Supplementary Material for details](#)) [50]. By plotting the rate/[e] $^{\beta}$ ([e]= N_e) against **1** using different tested values of rate, β can be identified when the two curves overlay [51,52]. The best fits give $\beta_{\text{C–O}}$ and β_{H} of 0.03 and 1.5, respectively ([Fig. S16](#)).

For coupling, the positive order in **1** suggests oxidative addition of aryl halide to Ni^{I} as the rate-determining step (RDS), which is consistent with that proposed for C–N/C–O coupling in analogue Ni/photoredox catalysis [11,42,45]. For hydrodehalogenation, the low substrate dependency and β_{H} of 1.5 imply the association of aryl halide at Ni (e.g. Ni^{I}), followed by a rate-limiting Ni-mediated electron transfer (an overall $2\text{e}^-/1\text{H}^+$ process, with electrons from CN support and proton from methanol hydroxyl group). Considering the approximation in data processing and complexity of heterogeneous catalysis, we do not intend to overstate this fractional reaction order in CN electron. Nonetheless, our rate law analysis affirms the difference in key elemental steps of the two conversions, and the significance of Ni_1/CN mediated electron transfer for hydrodehalogenation.

$$r = k[\mathbf{1}]^{\alpha} [e]^{\beta} \quad (3)$$

$$r = k' [\mathbf{1}]^{\alpha} \quad (3a)$$

$$\ln r = \alpha \ln([\mathbf{1}]) + \ln k' \quad (3b)$$

$$r' = \frac{\text{rate}}{[e]^{\beta}} = k[\mathbf{1}]^{\alpha} \quad (3c)$$

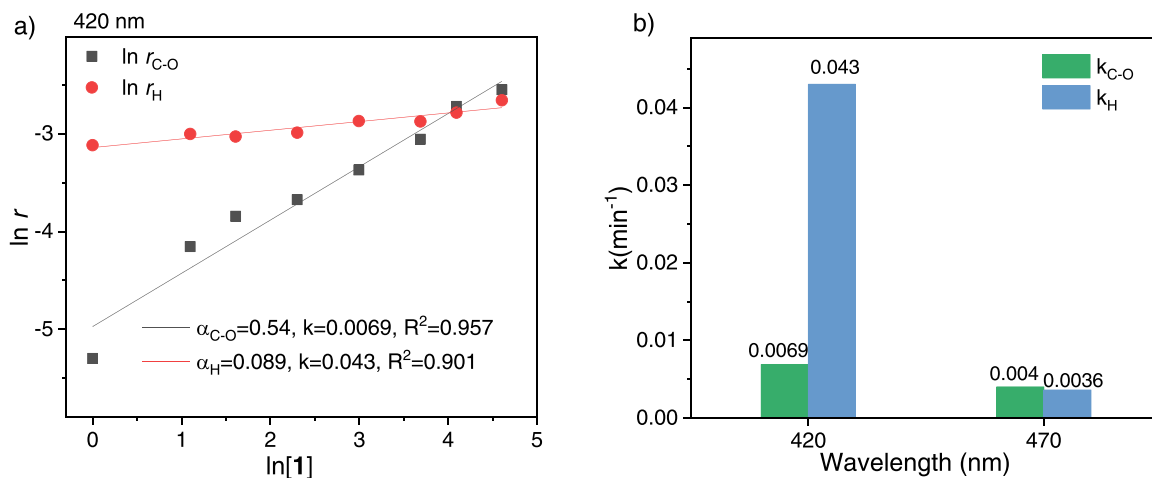


Fig. 5. (a) The logarithmic initial rates of coupling ($\ln r_{C-O}$) and dehalogenation ($\ln r_H$) were plotted against $\ln [1]$ under irradiation of 420 nm (100 mW cm⁻²). (b) The apparent rate constants (k) at 420 nm and 470 nm extracted from Fig. S13. Conditions: 10 mg Ni_1/CN , NaOH (0.2 M) in CH_3OH solution (5 mL), at 40 °C under Ar.

With the collected results shown above, the Ni_1/CN catalyzed conversion of aryl halide is schematically illustrated in Fig. 6. In addition to C-O coupling pathway initiated by photogenerated Ni^{I} in Ni_1/CN , the hydrodehalogenation via Ni mediated (CN) electron-proton transfer pathway is uncovered. In line with previously proposed mechanism, C-O coupling is mediated by Ni^{I} via self-sustained OA/RE ($\text{Ni}^{\text{I}}/\text{Ni}^{\text{III}}$ cycle), and the RDS are the oxidative addition of aryl halide to Ni^{I} , showing positive reaction order in aryl halide. In addition, the electron storage/transfer over semiconducting CN (accompanied by proton adsorption/intercalation [41,53]) pave the path for hydrodehalogenation via electron-proton transfer. The positive correlation between hydrodehalogenation yield and density of available electron (regulated by

photo flux/energy) on CN, as well as the value of β_H evince the key role of CN as electron(proton) feedstock in steering the metal-photocatalytic pathway. The mechanism of hydrodehalogenation on Ni_1/CN resembles that adopted by Cob(I)alamin based natural dehalogenases and single atom cobalt electrocatalysts dispersed on nitrogen doped carbon/carbon doped boron nitride support, where electron (together with proton) is pumped continuously from Fe-S cofactors/amino acid residues, or from cathodes/electrolyte [9,54]. Specifically, the rate of coupling was relatively slow at lower aryl bromide concentration, thus the rate of dehalogenation surpassed it when electron density on Ni_1/CN was high, leading to the inverse in product distribution shown in Fig. 2. Increase in irradiation power/intensity would

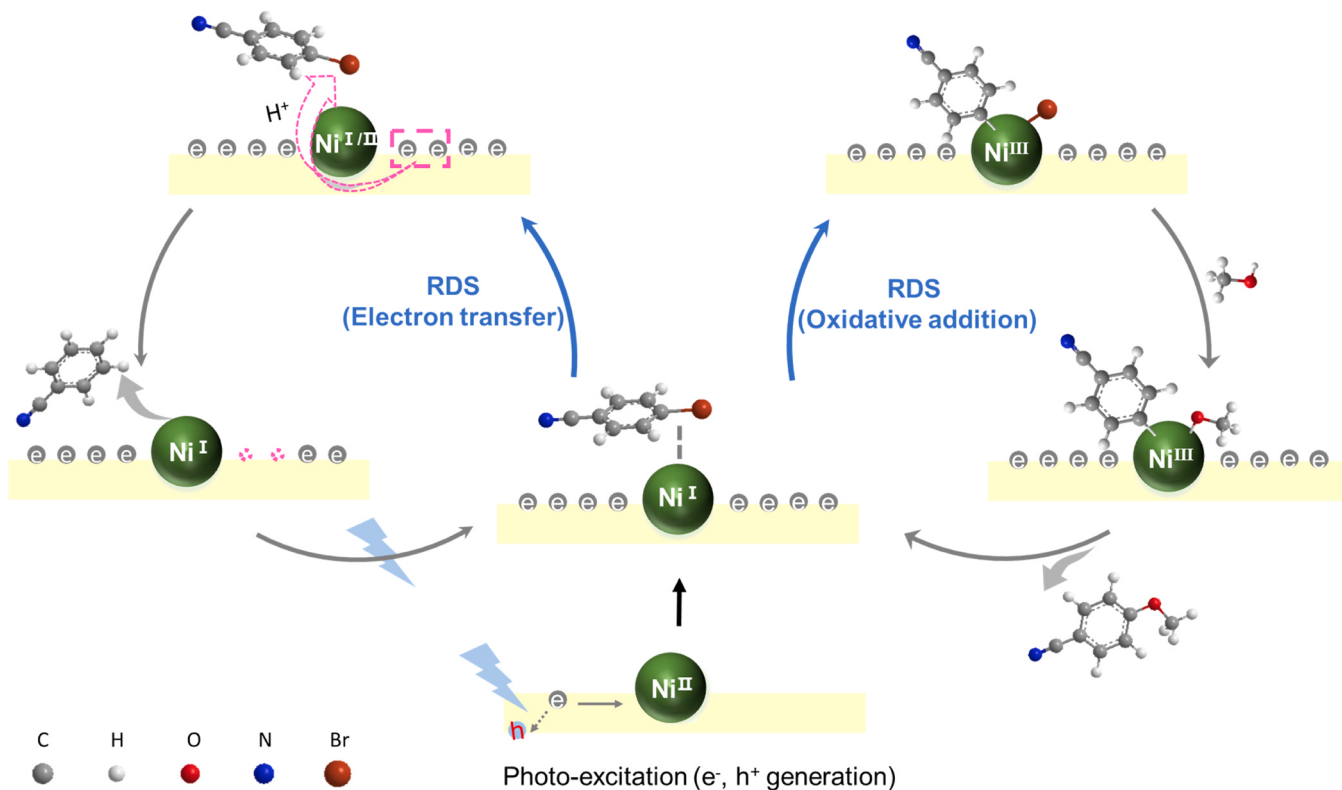


Fig. 6. The reaction pathway for dehalogenation and coupling over Ni_1/CN . The proposed mechanism for dehalogenation and coupling reaction catalyzed by Ni_1/CN .

favor generation of Ni^{I} , which benefits both conversions. However, coupling (with oxidative addition as RDS) undergoes redox neutral $\text{Ni}^{\text{I}}/\text{Ni}^{\text{III}}$ dark cycle, showing less sensitivity to irradiation condition (nearly-zero $\beta_{\text{C-O}}$ and substrate concentration dependence in the dark, Fig. S9b); while hydrodehalogenation involves rate-limiting electron transfer (eliminating the electron and Ni^{I}) and a higher β_{H} of 1.5, giving rise to a more pronounced change in hydrodehalogenation with the irradiation conditions (Fig. 2d-f). It is proposed that the interaction of aryl halide with Ni^{I} initiates the reaction, and the two conversions diverge from the follow-up steps, either the neutral OA/RE cycle to afford coupling product, or electron transfer (coupled with proton) toward hydrodehalogenation (consuming both the electron and Ni^{I}). It is acknowledged that this process may experience Ni intermediates with different oxidation state, however, due to the lack of further experimental evidence, the dehalogenation pathway shown here is simplified.

4. Conclusion

To conclude, we have unveiled Ni_1/CN catalyzed kinetically competitive C–O coupling and hydrodehalogenation. At high concentration of aryl halides/lower photo flux, C–O coupling dominate the reaction, while hydrodehalogenation works in a contrasting fashion. The involvement of photogenerated active specie (Ni^{I} and photoinduced electrons on CN) were affirmed by EPR spectroscopy and electron titration. The distinct kinetic behaviors/raw-law are on account of their different rate-determining steps: the dehalogenation/coupling shows the reaction orders of 0.1/0.5 in aryl halide and 1.5/0.03 in (CN) electron, respectively. The C–O coupling occurs via rate limiting OA of aryl halide to Ni^{I} (OA/RE ($\text{Ni}^{\text{I}}/\text{Ni}^{\text{III}}$) cycle), whereas hydrodehalogenation proceed via a rate-limiting (Ni mediated) electron transfer, originating from the unique electron-accumulation/transfer property of CN support (electron-proton transfer process). Our study illustrates mechanistic insights into the light-driven single site nickel catalytic aryl halide conversions, and signify the potential of photocatalytic support in regulation reactivity by storing/transferring electrons.

CRediT authorship contribution statement

Bangrong Ming: Visualization, Writing-original draft, Investigation, Methodology. **Tongtong Jia:** Methodology. **Yufan Zhang:** Methodology. **Jikun Li:** Funding acquisition, Methodology. **Chuncheng Chen:** Funding acquisition, Methodology, Supervision. **Wenjing Song:** Funding acquisition, Methodology, Project administration, Supervision, Writing-review & editing. **Jincai Zhao:** Funding acquisition, Methodology, Supervision.

Declaration of Competing Interest

The authors declare that they have no known competing financial interests or personal relationships that could have appeared to influence the work reported in this paper.

Data availability

Data will be made available on request.

Acknowledgements

This work was supported by the “National Key Research and Development Program of China” (Nos. 2022YFA1205603 and 2019YFA0210401), the National Natural Science Foundation of China (Nos. 22076194, 22188102, and 22273111), and the Strategic Priority Research Program of Chinese Academy of Sciences, Grant No. XDB36000000.

Appendix A. Supplementary data

Supplementary material related to this article can be found, in the online version.

Appendix B. Supporting information

Supplementary data associated with this article can be found in the online version at doi:10.1016/j.apcatb.2023.123653.

References

- [1] J. Twilton, C. Le, P. Zhang, M.H. Shaw, R.W. Evans, D.W.C. MacMillan, The merger of transition metal and photocatalysis, *Nat. Rev. Chem.* 1 (2017) 0052.
- [2] C.-S. Wang, P.H. Dixneuf, J.-F. Soulé, Photoredox catalysis for building C–C bonds from $\text{C}(\text{sp}^2)\text{-H}$ bonds, *Chem. Rev.* 118 (2018) 7532–7585.
- [3] K. Li, B.S. Peng, T.Y. Peng, Recent advances in heterogeneous photocatalytic CO_2 conversion to solar fuels, *ACS Catal.* 6 (2016) 7485–7527.
- [4] K. Sun, Y.Y. Qian, H.L. Jiang, Metal-organic frameworks for photocatalytic water splitting and CO_2 reduction, *Angew. Chem., Int. Ed.* 62 (2023), e202217565.
- [5] M. Cybularczyk-Cecotka, J. Szczepanik, M. Giedyk, Photocatalytic strategies for the activation of organic chlorides, *Nat. Catal.* 3 (2020) 872–886.
- [6] J.A. Terrett, J.D. Cuthbertson, V.W. Shurtliff, D.W.C. MacMillan, Switching on elusive organometallic mechanisms with photoredox catalysis, *Nature* 524 (2015) 330–334.
- [7] D.M. Schultz, T.P. Yoon, Solar synthesis: prospects in visible light photocatalysis, *Science* 343 (2014) 1239176.
- [8] H. Qin, T. Zha, K. Qian, Y. Sun, X. Guan, C. Chen, Efficient full dechlorination of chlorinated ethenes on single enzyme-like $\text{Co}-\text{N}_4$ sites in nitrogen-doped carbons, *Appl. Catal. B-Environ.* 328 (2023), 122459.
- [9] C. Kunze, M. Bommmer, W.R. Hagen, M. Uksa, H. Dobbek, T. Schubert, G. Diekert, Cobamide-mediated enzymatic reductive dehalogenation via long-range electron transfer, *Nat. Commun.* 8 (2017) 15858.
- [10] L. Yang, H.H. Lu, C.H. Lai, G. Li, W. Zhang, R. Cao, F.Y. Liu, C. Wang, J.L. Xiao, D. Xue, Light-promoted nickel catalysis: etherification of aryl electrophiles with alcohols catalyzed by a $\text{Ni}^{\text{II}}\text{-Aryl}$ complex, *Angew. Chem. Int. Ed.* 59 (2020) 12714–12719.
- [11] S.I. Ting, W.L. Williams, A.G. Doyle, Oxidative addition of aryl halides to a $\text{Ni}(\text{I})$ -bipyridine complex, *J. Am. Chem. Soc.* 144 (2022) 5575–5582.
- [12] B.J. Shields, A.G. Doyle, Direct $\text{C}(\text{sp}^3)\text{-H}$ cross coupling enabled by catalytic generation of chlorine radicals, *J. Am. Chem. Soc.* 138 (2016) 12719–12722.
- [13] H. Shimakoshi, Y. Hisaeda, Oxygen-controlled catalysis by vitamin B12– TiO_2 : formation of esters and amides from trichlorinated organic compounds by photoirradiation, *Angew. Chem. Int. Ed.* 54 (2015) 15439–15443.
- [14] L. Ji, C.C. Wang, S.J. Ji, K.P. Keppler, P. Paneth, Mechanism of cobalamin-mediated reductive dehalogenation of chloroethylenes, *ACS Catal.* 7 (2017) 5294–5307.
- [15] E.R. Welin, C. Le, D.M. Arias-Rotondo, J.K. McCusker, D.W.C. MacMillan, Photosensitized, energy transfer-mediated organometallic catalysis through electronically excited nickel(II), *Science* 355 (2017) 380–385.
- [16] K.X. Wang, H.T. Jiang, H.L. Liu, H.Y. Chen, F. Zhang, Accelerated direct hydroxylation of aryl chlorides with water to phenols via the proximity effect in a heterogeneous metallaphotocatalyst, *ACS Catal.* 12 (2022) 6068–6080.
- [17] T.J. Liu, C.Y. Deng, D. Meng, Y.F. Zhang, R. Duan, H.W. Ji, H. Sheng, J.K. Li, C. C. Chen, J.C. Zhao, W.J. Song, Aligning metal coordination sites in metal-organic framework-enabled metallaphotoredox catalysis, *ACS Appl. Mater. Interfaces* 15 (2023) 5139–5147.
- [18] J. Lee, W.J. Song, Photocatalytic C–O coupling enzymes that operate via intramolecular electron transfer, *J. Am. Chem. Soc.* 145 (2023) 5211–5221.
- [19] S. Liu, Y. Hu, H. Xu, Z. Lou, J. Chen, C.-Z. Yuan, X. Lv, X. Duan, S. Wang, X.-L. Wu, Directional electron transfer in single-atom cobalt nanzyme for enhanced photo-Fenton-like reaction, *Appl. Catal. B-Environ.* 335 (2023), 122882.
- [20] X.X. Jin, R.Y. Wang, L.X. Zhang, R. Si, M. Shen, M. Wang, J.J. Tian, J.L. Shi, Electron Configuration Modulation of Nickel Single Atoms for Elevated Photocatalytic Hydrogen, *Evol. Angew. Chem. Int. Ed.* 59 (2020) 6827–6831.
- [21] C. Cavedon, S. Gisbertz, S. Reischauer, S. Vogl, E. Sperlich, J.H. Burke, R. Wallick, S. Schrottke, W.H. Hsu, L. Anghileri, Y. Pfeifer, N. Richter, C. Teutloff, H. Muller-Werkmeister, D. Cambie, P.H. Seeger, J. Vura-Weis, R.M. van der Veen, A. Thomas, B. Pieber, Intraligand charge transfer enables visible-light-mediated nickel-catalyzed cross-coupling reactions, *Angew. Chem., Int. Ed.* 61 (2022), e202211433.
- [22] Y.Z. Zhang, C. Liang, H.P. Feng, W. Liu, Nickel single atoms anchored on ultrathin carbon nitride for selective hydrogen peroxide generation with enhanced photocatalytic activity, *Chem. Eng. J.* 446 (2022), 137379.
- [23] M. Kwak, J. Bok, B.H. Lee, J. Kim, Y. Seo, S. Kim, H. Choi, W. Ko, W.H. Antink, C. W. Lee, G.H. Yim, H. Seung, C. Park, K.S. Lee, D.H. Kim, T. Hyeon, D. Yoo, Ni single atoms on carbon nitride for visible-light-promoted full heterogeneous dual catalysis, *Chem. Sci.* 13 (2022) 8536–8542.
- [24] L.Z. Xing, Q. Yang, C. Zhu, Y.L. Bai, Y.R. Tang, M. Rueping, Y.F. Cai, Poly(heptazine imide) ligand exchange enables remarkable low catalyst loadings in heterogeneous metallaphotocatalysis, *Nat. Commun.* 14 (2023) 1501.

[25] A. Vijeta, C. Casadevall, S. Roy, E. Reisner, Visible-light promoted C–O bond formation with an integrated carbon nitride–nickel heterogeneous photocatalyst, *Angew. Chem. Int. Ed.* 60 (2021) 8494–8499.

[26] X. Zhao, C.Y. Deng, D. Meng, H.W. Ji, C.C. Chen, W.J. Song, J.C. Zhao, Nickel-coordinated carbon nitride as a metallaphotoredox platform for the cross-coupling of aryl halides with alcohols, *ACS Catal.* 10 (2020) 15178–15185.

[27] S. Gisbertz, S. Reischauer, B. Pieber, Overcoming limitations in dual photoredox–nickel-catalysed C–N cross-couplings due to catalyst deactivation, *Nat. Catal.* 3 (2020) 611–620.

[28] R. Godin, Y. Wang, M.A. Zwijnenburg, J.W. Tang, J.R. Durrant, Time-resolved spectroscopic investigation of charge trapping in carbon nitrides photocatalysts for hydrogen generation, *J. Am. Chem. Soc.* 139 (2017) 5216–5224.

[29] D.S. Zhang, P.J. Ren, W.W. Liu, Y.R. Li, S. Salli, F.Y. Han, W. Qiao, Y. Liu, Y.Z. Fan, Y. Cui, Y.B. Shen, E. Richards, X.D. Wen, M.H. Rummeli, Y.W. Li, F. Besenbacher, H. Niemantsverdriet, T.B. Lim, R. Su, Photocatalytic abstraction of hydrogen atoms from water using hydroxylated graphitic carbon nitride for hydrogenative coupling reactions, *Angew. Chem. Int. Ed.* 61 (2022), e202204256.

[30] Q. Wang, G.G. Zhang, W.D. Xing, Z.M. Pan, D.D. Zheng, S.B. Wang, Y.D. Hou, X. C. Wang, Bottom-up synthesis of single-crystalline poly(triazine imide) nanosheets for photocatalytic overall water splitting, *Angew. Chem. Int. Ed.* 62 (2023), e202307930.

[31] J.N. Schrauben, R. Hayoun, C.N. Valdez, M. Braten, L. Fridley, J.M. Mayer, Titanium and zinc oxide nanoparticles are proton-coupled electron transfer agents, *Science* 336 (2012) 1298–1301.

[32] P. Huang, J. Huang, S.A. Pantovich, A.D. Carl, T.G. Fenton, C.A. Caputo, R. L. Grimm, A.I. Frenkel, G. Li, Selective CO₂ reduction catalyzed by single cobalt sites on carbon nitride under visible-light irradiation, *J. Am. Chem. Soc.* 140 (2018) 16042–16047.

[33] Y.Z. Zhang, C. Liang, H.P. Feng, W. Liu, Nickel single atoms anchored on ultrathin carbon nitride for selective hydrogen peroxide generation with enhanced photocatalytic activity, *Chem. Eng. J.* 446 (2022), 137379.

[34] Y. Hou, Y.-L. Liang, P.-C. Shi, Y.-B. Huang, R. Cao, Atomically dispersed Ni species on N-doped carbon nanotubes for electroreduction of CO₂ with nearly 100 % CO selectivity, *Appl. Catal. B-Environ.* 271 (2020), 118929.

[35] L. Cheng, H. Yin, C. Cai, J.J. Fan, Q.J. Xiang, Single Ni atoms anchored on porous few-layer g-C₃N₄ for photocatalytic CO₂ reduction: the role of edge confinement, *Small* 16 (2020) 2002411.

[36] J.H. Lan, R.X. Chen, F.F. Duo, M.H. Hu, X.Y. Lu, Visible-light photocatalytic reduction of aryl halides as a source of aryl radicals, *Molecules* 27 (2022) 5364.

[37] G.M. Liu, Y. Huang, H.Q. Lv, H. Wang, Y.B. Zeng, M.Z. Yuan, Q.G. Meng, C. Y. Wang, Confining single-atom Pd on g-C₃N₄ with carbon vacancies towards enhanced photocatalytic NO conversion, *Appl. Catal. B-Environ.* 284 (2021), 119683.

[38] P. Xia, B. Cheng, J. Jiang, H. Tang, Localized π -conjugated structure and EPR investigation of g-C₃N₄ photocatalyst, *Appl. Surf. Sci.* 487 (2019) 335–342.

[39] O. Trofanchuk, M. Stein, C. Gessner, F. Lendzian, Y. Higuchi, W. Lubitz, Single crystal EPR studies of the oxidized active site of [NiFe] hydrogenase from *Desulfovibrio vulgaris Miyazaki F*, *J. Biol. Inorg. Chem.* 5 (2000) 36–44.

[40] S. Xu, E.D. Walter, Z. Zhao, M.Y. Hu, X. Han, J.Z. Hu, X. Bao, Dynamic structural changes of SiO₂ supported Pt–Ni bimetallic catalysts over redox treatments revealed by NMR and EPR, *J. Phys. Chem. C* 119 (2015) 21219–21226.

[41] T.T. Jia, D. Meng, R. Duan, H.W. Ji, H. Sheng, C.C. Chen, J.K. Li, W.J. Song, J. C. Zhao, Single-atom nickel on carbon nitride photocatalyst achieves semihydrogenation of alkynes with water protons via monovalent nickel, *Angew. Chem., Int. Ed.* 62 (2023), e202216511.

[42] H. Na, L.M. Mirica, Deciphering the mechanism of the Ni-photocatalyzed C–O cross-coupling reaction using a tridentate pyridinophane ligand, *Nat. Commun.* 13 (2022) 1313.

[43] N.A. Till, L. Tian, Z. Dong, G.D. Scholes, D.W.C. MacMillan, Mechanistic analysis of metallaphotoredox C–N coupling: photocatalysis initiates and perpetuates Ni(I)/Ni(III) coupling, *Acta. J. Am. Chem. Soc.* 142 (2020) 15830–15841.

[44] C.S. Day, A. Renteria-Gomez, S.J. Ton, A.R. Gogoi, O. Gutierrez, R. Martin, Elucidating electron-transfer events in polypyridine nickel complexes for reductive coupling reactions, *Nat. Catal.* 6 (2023) 244–253.

[45] R. Sun, Y.Z. Qin, S. Ruccolo, C. Schnedermann, C. Costentin, D.G. Nocera, Elucidation of a redox-mediated reaction cycle for nickel-catalyzed cross coupling, *J. Am. Chem. Soc.* 141 (2019) 89–93.

[46] Y.Y. Wang, Q. Zhu, Y. Wei, Y.J. Gong, C.C. Chen, W.J. Song, J.C. Zhao, Catalytic hydrodehalogenation over supported gold: electron transfer versus hydride transfer, *Appl. Catal. B-Environ.* 231 (2018) 262–268.

[47] I. Ghosh, T. Ghosh, J.I. Bardagi, B. Konig, Reduction of aryl halides by consecutive visible light-induced electron transfer processes, *Science* 346 (2014) 725–728.

[48] Y. Yan, W.D. Shi, Z. Yuan, S.G. He, D.M. Li, Q.B. Meng, H.W. Ji, C.C. Chen, W. H. Ma, J.C. Zhae, The formation of Ti–H species at interface is lethal to the efficiency of TiO₂-based dye-sensitized Devices, *J. Am. Chem. Soc.* 139 (2017) 2083–2089.

[49] J.A. Malik, A. Madani, B. Pieber, P.H. Seeberger, Evidence for photocatalyst involvement in oxidative additions of nickel-catalyzed carboxylate O-arylations, *J. Am. Chem. Soc.* 142 (2020) 11042–11049.

[50] C.D.T. Nielsen, J. Bures, Visual kinetic analysis, *Chem. Sci.* 10 (2019) 348–353.

[51] J.M. Koelewijn, M. Lutz, W.I. Dzik, R.J. Detz, J.N.H. Reek, Reaction progress kinetic analysis as a tool to reveal ligand effects in Ce(IV)-Driven IrCp⁺-catalyzed water oxidation, *ACS Catal.* 6 (2016) 3418–3427.

[52] J.S. Mathew, M. Klussmann, H. Iwamura, F. Valera, A. Futran, E.A.C. Emanuelsson, D.G. Blackmond, Investigations of Pd-catalyzed ArX coupling reactions informed by reaction progress kinetic analysis, *J. Org. Chem.* 71 (2006) 4711–4722.

[53] J. Yang, W. Liu, M. Xu, X. Liu, H. Qi, L. Zhang, X. Yang, S. Niu, D. Zhou, Y. Liu, Y. Su, J.-F. Li, Z.-Q. Tian, W. Zhou, A. Wang, T. Zhang, Dynamic behavior of single-atom catalysts in electrocatalysis: identification of Cu-N3 as an active site for the oxygen reduction reaction, *J. Am. Chem. Soc.* 143 (2021) 14530–14539.

[54] Y. Min, X. Zhou, J.J. Chen, W.X. Chen, F.Y. Zhou, Z.Y. Wang, J. Yang, C. Xiong, Y. Wang, F.T. Li, H.Q. Yu, Y.E. Wu, Integrating single-cobalt-site and electric field of boron nitride in dechlorination electrocatalysts by bioinspired design, *Nat. Commun.* 12 (2021) 303.